frontiers in Physics

ORIGINAL RESEARCH
published: 05 February 2020
doi: 10.3389/fphy.2020.00013

Medical Applications of Tissue-Equivalent, Organic-Based Flexible Direct X-Ray Detectors

Laura Basiricò[1,2], Andrea Ciavatti[1,2], Ilaria Fratelli[1,2], Diego Dreossi[3], Giuliana Tromba[3], Stefano Lai[4], Piero Cosseddu[4], Annalisa Bonfiglio[4], Francesco Mariotti[5], Carlo Dalla Val[5], Valerio Bellucci[6], John E. Anthony[7] and Beatrice Fraboni[1,2]*

[1] Department of Physics and Astronomy, University of Bologna, Bologna, Italy, [2] National Institute of Nuclear Physics (INFN), Section of Bologna, Bologna, Italy, [3] Elettra-Sincrotrone Trieste, Trieste, Italy, [4] Department of Electrical and Electronic Engineering, University of Cagliari, Cagliari, Italy, [5] Skan-X Radiology Devices S.p.A., Bologna, Italy, [6] Skanray Europe S.r.l., Bologna, Italy, [7] Center for Applied Energy Research, University of Kentucky, Lexington, KY, United States

The aim of this study is to assess direct X-ray detectors based on organic thin films, fabricated onto flexible plastic substrates, and operating at ultra-low bias (<1 V), for different medical applications. With this purpose, flexible fully organic pixelated X-ray detectors have been tested at the imaging beamline SYRMEP (SYnchrotron Radiation for MEdical Physics) at the Italian synchrotron Elettra, Trieste. The detectors' performance has been assessed for potential employment both as reliable wearable personal dosimeters for patients and as flexible X-ray medical imaging systems. A spatial resolution of 1.4 lp mm^{-1} with a contrast of 0.37 has been evaluated. Finally, we validate the detector using X-ray doses and energies typically employed for actual medical radiography, and using X-ray beam pulses provided by a commercial dental radiography system, recording a sensitivity of 1.6×10^5 $\mu C\ Gy^{-1}\ cm^{-3}$ with a linear response with increasing of the dose rates and a reliable signal to 100 ms X-rays pulses.

Keywords: organic X-ray detectors, wearable electronics, flexible electronics, thin films, medical dosimetry

OPEN ACCESS

Edited by:
Christer Frojdh, Mid Sweden University, Sweden

Reviewed by:
Giovanni Paternoster, Fondazione Bruno Kessler, Italy
Gabriele Giacomini, Brookhaven National Laboratory (DOE), United States

****Correspondence:***
Laura Basiricò
laura.basirico2@unibo.it

Specialty section:
This article was submitted to Radiation Detectors and Imaging, a section of the journal Frontiers in Physics

Received: *18 September 2019*
Accepted: *14 January 2020*
Published: *05 February 2020*

Citation:
Basiricò L, Ciavatti A, Fratelli I, Dreossi D, Tromba G, Lai S, Cosseddu P, Bonfiglio A, Mariotti F, Dalla Val C, Bellucci V, Anthony JE and Fraboni B (2020) Medical Applications of Tissue-Equivalent, Organic-Based Flexible Direct X-Ray Detectors. Front. Phys. 8:13. doi: 10.3389/fphy.2020.00013

INTRODUCTION

Nowadays, the employment of ionizing radiation sources (X- and gamma-rays, protons, electrons) for medical diagnostic, monitoring, and therapy is widespread and is continuously expanding. As a consequence, there is a growing interest in the development of novel materials and devices suitable for ionizing radiation detection for medical application. Indeed, personal dosimeters commercially available are rigid and uncomfortable to be worn or placed in the vicinity of the organ under examination. Further, most of the solid-state detectors employed for dosimetry cannot be considered tissue-equivalent due to their composition with heavy elements and their consequent high X-ray absorbing power, causing limited reliable calibration issues. Moreover, despite the tissue-equivalence requirement can be addressed by diamond-based X-ray dosimeters [1], these devices still present high manufacturing costs for large area devices, similarly to other high performing detectors based on inorganic highly pure single crystals or films. Concerning commercial imaging flat panels, typically based on a-Si, a-Se, or poly-CZT, they are heavy, bulky, difficult to grow in large pixelated matrices with limited costs and by means of easy and low-temperature fabrication techniques and maintain the stiff mechanical properties of the materials employed in medical dosimetry. In this framework, organic semiconductors, i.e., organic small

molecules and polymers, are very promising innovative materials for the active layer of both direct [2–7] and indirect [8, 9] ionizing radiation detection systems, since they possess unique properties which make them suitable for this application. First of all, they are easily processable in liquid phase and thus can be deposited by means of low-cost techniques (e.g., blade coating [10], spray coating [11], inkjet printing [12]) at low temperature onto unconventional flexible and conformable substrates, as polyethylene terephthalate (PET), polyethylene naphthalate (PEN), polyimide (Kapton) foils and even synthetic and natural textiles, and therefore particularly convenient for wearable electronics. Moreover, since their main components are hydrogen and carbon, organic semiconductors are characterized by a low atomic number, similar to the average human tissue-equivalent Z and this makes them ideal candidates for accurate and reliable real-time *in situ* dosimetry. In fact, if from the one side their low radiation absorption (i.e., the material quantum efficiency) could be considered a limitation, from the other side, it allows direct measurement of the actual impinging radiation dose in the target point. In other words, they can be interposed between the X-ray source and the patient without significantly absorbing the impinging beam. For these reasons in the last 10 years several and varied works on organic-based X- and gamma-ray detectors have been reported in literature. Indeed, organic semiconductors have been employed in indirect detectors both as scintillators [13–15] and as active layer of photodiodes [16, 17], and in direct detectors in form of single crystals [18–22] and thin films [23–26]. Among these reports, few present devices operating at low voltages and fabricated on flexible and lightweight substrates, able to envisage their employment as wearable sensors for medical application, and none of them demonstrated so far X-ray imaging without the employment of Si-TFTs matrix backplane. Moreover, most of these works, with the aim to increase the attenuated fraction of the devices, propose blending of the organic semiconductors with high-Z elements (metallic and oxide nanoparticles [27–29], lead-based quantum dots [30]) which however lose the tissue-equivalence of organic materials and, over a certain concentration, can negatively affect the transport properties and the stability of the active layer. More recently, thin film lead-halide perovskite devices have been proposed as alternative highly absorbing material for low-voltage and (potentially) flexible X-ray detectors [31–33]. However, they suffer from instability issues and, even with such materials, the tissue-equivalence is not targeted. Furthermore, the presence of lead, i.e., a certain level of toxicity, makes them inconvenient for medical and wearable sensors, where the devices must get in contact with the human body.

Recently, our group demonstrated how all organic thin films (100–200 nm thick) deposited from solution onto interdigitated electrodes on flexible PET foil, are able to detect X-rays at ultra-low bias (<1 V) and with a high sensitivity (up to 9.0×10^5 $\mu C\ Gy^{-1}\ cm^{-3}$) thanks to a trap-assisted photoconductive gain detection mechanism [25, 34]. This is the record sensitivity for solid-state organic X-ray detectors and the corresponding value per unit area (12.3 $\mu C\ Gy^{-1}\ cm^{-2}$) is competitive with some of the inorganic materials currently used to fabricate large-area detectors (amorphous selenium has typical values of 25 $\mu C\ Gy^{-1}\ cm^{-2}$) [35]. The highest value reported in literature for hybrid organic-inorganic X-ray detector is that of Thirimanne et al. [23], with $1.7 \cdot 10^6$ $\mu C\ Gy^{-1}\ cm^{-3}$ sensitivity for devices with vertical diode architecture where a bulk heterojunction-nanoparticles (BHJ-NP) composite is sandwiched between indium tin oxide (ITO) and aluminum (Al) electrodes. However, as already mentioned, the presence of heavy inorganic nanoparticles makes such devices not tissue equivalent as the here tested full-organic detectors. Considering the other full-organic X-ray detectors reported in literature, the sensitivity of the here reported X-ray full-organic detector exceeds by several orders of magnitude those for devices based on thin polymeric films [6, 24, 36] or bulk organic single crystals [3, 18], biased at several tens of volts. To the best of our knowledge, no other full-organic X-ray detectors have been reported in literature so far. In this work, we demonstrate the potentiality of such full-organic flexible detectors as medical diagnostic (e.g., as bone density analyzer) and dosimetry (e.g., for mammography) tools, giving also the proof of principle for their application as X-ray imagers with a linear response at low dose rates and the ability to follow X-rays pulses of 100 ms. To reach this goal, we tested the detectors in relevant environments for medical analysis: a synchrotron beamline conceived and equipped to test X-ray imaging systems (i.e., monochromatic X-ray beam tunable in energy and shape) and a commercial dental X-ray radiographic system. To the best of our knowledge, this is the first report on the validation and testing under actual clinical environment of a full organic (tissue-equivalent) wearable X-ray medical sensor.

MATERIALS AND METHODS

The detector under test is 4-pixels array with four single reading channels and one common biased electrode (**Figure 1a**). Each pixel of the 4-pixel array detector is a X-rays photoresistor, with an area of $4 \times 4\ mm^2$ and interdigitated electrodes structure (channel length, i.e., the distance between two gold "fingers" of the interdigitated structure is $L = 30 \pm 5\,\mu m$, channel width, i.e., the total length of the interdigitated electrodes, is $W = 45 \pm 1\,mm$). The pitch between the pixels is 4.3 mm. The gold electrodes were patterned by means of standard photolithography from a unique, 80 nm thick gold layer, deposited by thermal evaporation at room temperature and in high vacuum conditions (5×10^{-5} Torr) onto flexible 175 μm thick PET substrate. Gold has been employed as electrodes material since it forms ohmic contacts with TIPS-pentacene, i.e., ensuring an efficient injection/collection of charges to/from the organic semiconductor, being the work function of gold $\phi_{Au} = (5.31 \div 5.37)$ eV [37] generally considered matching to HOMO (Highest Occupied Molecular Orbital) level of TIPS-pentacene ($\phi_{TIPS} = 5.3$ eV) [38]. The organic active layer is 100–200 nm thick and two different organic small molecules have been employed: 6,13-bis(triisopropylsilylethynyl)pentacene (TIPS-pentacene) and bis(triisopropylgermylethynyl) pentacene (TIPGe-pentacene) i.e., the same molecule structure where the two Si atoms are substituted by Ge atoms. Devices based on both the semiconductor layers have recently demonstrated high

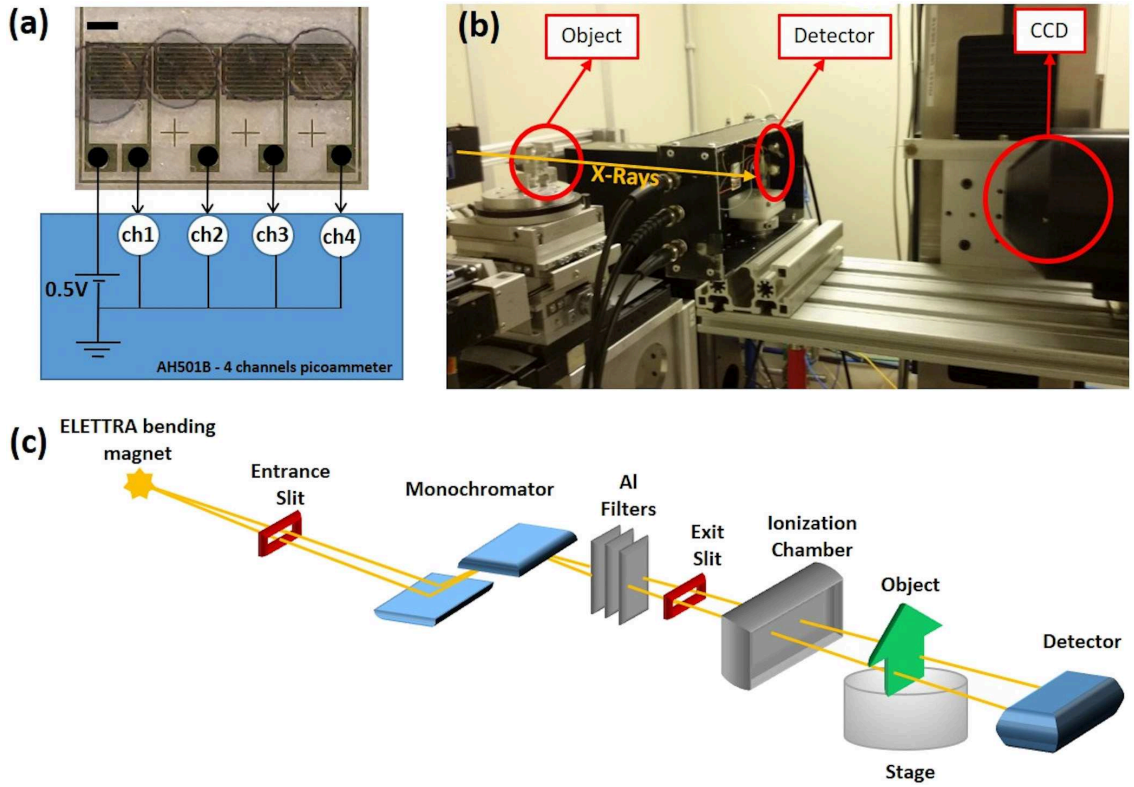

FIGURE 1 | (a) Picture of the 4 pixels-array organic thin film detector employed in this work (the scale bar is 2 mm) and the electrical circuit used for the signals acquisition (4-channels AH50b picoammeter) and the biasing of the detector (each pixel at 0.5V). Image **(b)** and schematic **(c)** of the experimental setup in SYRMEP beamline: the X-ray beam hits the object placed onto a motorized stage; the detector is mounted behind it in a Faraday Cage to minimize electrical noise; a CCD camera allows to properly align the object and the detector. The dark yellow arrow/line represents the X-ray beam.

sensitivity for the ionizing radiation detection [6, 25, 26, 34, 39]. The organic semiconductor-based solutions were prepared at 0.5 wt.% concentration in toluene, stirred at 80°C for 1 h and then deposited by drop casting onto interdigitated gold electrodes keeping the substrate heated at 60°C and covered with a glass cup to enhance crystallization. After the deposition the devices were annealed at 80°C for 1 h. The working principle of the device described above is that typical of an X-ray photoconductive detector. When a voltage is applied through the contacts, an intrinsic current, due to the free carriers concentration (assumed of only one kind), flows in the semiconductor layer. When the X-rays impinges onto the device, the carrier concentration increases resulting in an increase of the semiconductor conductivity and the photocurrent amplitude will be proportional to the radiation dose rate [40]. The assumption of the transport of only one kind of charge carriers (holes in the case of TIPS-pentacene), implies that the others (electrons) are deeply trapped in the semiconductor. With ohmic contacts, charge neutrality is guaranteed in the device, hence for every collected hole another one will be injected, until a recombination with a trapped electron occurs. Since more than one hole can flow in consequence of a single absorbed photon, a detection external efficiency higher than 100% is possible [16], ruled by the ratio between the electron/hole recombination time and the hole transit time, which is called photoconductive gain [25]. Such a gain process makes possible the detection of high energy photons by such low-Z tissue equivalent materials, which internal quantum efficiency is extremely low due to the limited radiation absorption (e.g., 0.015% for 100nm thick TIPS-pentacene device irradiated with X-ray at 17 keV). The detector structure is shown in a picture in **Figure 1a** together with the electrical circuit employed for the signals acquisition. All the characterizations under X-rays were carried out at room temperature, in dark and placing the detector into a faraday cage to minimize the electromagnetic noise.

For the X-ray irradiation we employed different experimental setups, the first one used monochromatic X-rays delivered by a synchrotron facility, the others were based on conventional generators used for dental radiography:

1) The SYRMEP (Synchrotron Radiation for Medical Physics) beamline at ELETTRA, Trieste, has been chosen for this study since it is designed for research medical diagnostic radiology application, in particular with energies and dose rates typical of mammography [41]. Indeed, recently synchrotron radiation has been demonstrated as a powerful tool for clinical mammography thanks to its many advantages with respect to conventional X-ray tube systems [42]. In fact, its high fluxes (typically about 10^8

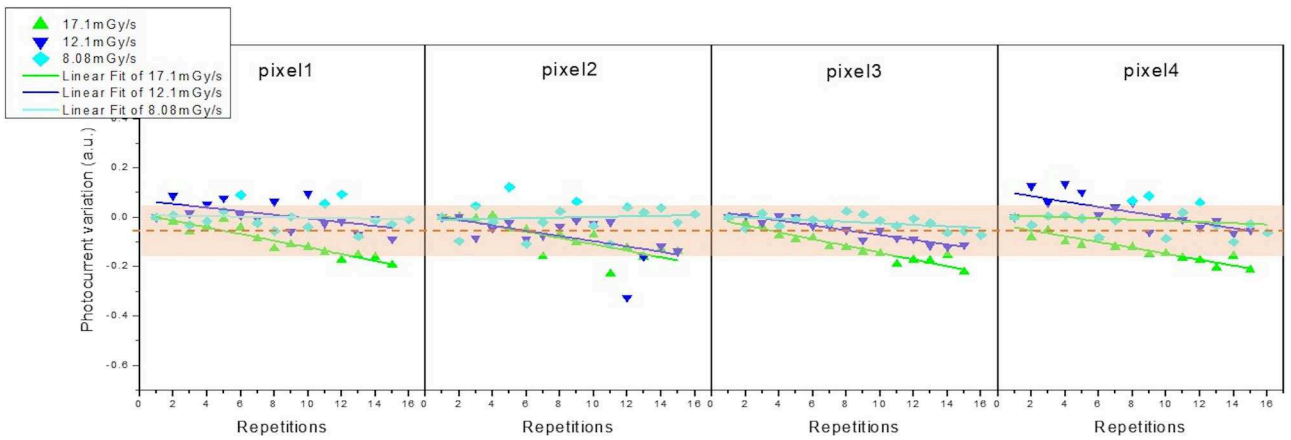

FIGURE 2 | Normalized signal amplitude variation of the four pixels measured for subsequent 15 repetitions of synchrotron X-rays on/off exposure cycles (2 s on and 10 s off) for different dose rates: 8.1, 12.1, and 17.1 mGy s^{-1}. The average variation is indicated by the orange dashed line while the orange band represents the error associated. The solid lines represent the linear fits of each set of data.

ph $mm^{-2}s^{-1}$) allow the selection of the most appropriate energy window with narrow bandwidth (0.1%). Also, the high spatial coherence enables phase-sensitive X-ray imaging techniques, improving radiographic diagnostic image quality. The SYRMEP monochromator, based on a double Si(1,1,1) crystal system working in Bragg configuration, provides a laminar section X-ray beam in the energy range between 8.5 and 35 keV, with energy resolution of 10^{-3} and dose rate in the range 0.05–35 mGy s^{-1}. The dose rates impinging on the sample can be varied by using five aluminum filters and real-time monitored by means of an ionization chamber. Thanks to the possibility to modulate the beam shape in a very precise region of the active layer and to control the area of irradiation by means of precision slits and a CCD camera, we could control the area and the position of irradiation within the detector. In **Figure 1b,** the picture of the experimental setup is reported: the signals were acquired while moving a phantom between the X-ray source and the detector, thanks to a sample stage equipped with translation stages. A schematic of the entire SYRMEP beamline is reported in **Figure 1c**. The CCD camera was placed after the detector and allowed the correct phantom/detector alignment, crucial for the success of this kind of measurements. During the measurements at SYRMEP electrical signals were simultaneously collected from the 4 pixels (biased at 0.5 V) through the 4-channel picoammeters AH501b (ELETTRA), capable to detect the current variations from each pixel and to real-time monitor the signal (**Figure 1a**).

2) A commercial W-target panoramic X-ray tube (OPX/105 Serial Number: 681502 by Skan-X Radiology Devices S.p.A), with a maximum operating voltage of 120 kVp, providing low irradiation dose down to about 5 μGy, the typical values for exposure during a dental radiography. The electrical measurements under this X-ray beam (without any filter) were carried out employing a Keithley 2614B source-meter unit. The dose rate range [15.5–64.6] μGy used for this work refers to the air kerma, and the values have been measured through a BARRACUDA X-Ray Analyzer from RTI Electronics.
3) Intraskan DC, a dental radiography system commercialized by Skanray Europe srl. This machine allows a 3 points control: 50–70 kVp voltage range, 4–8 mA anodic current range and time windows from several seconds to 10 ms. The electrical measurements under the Intraskan DC X-ray beam was performed without filtering the radiation, using a Keysight B2912A source-meter unit. Also in this case the dose rates [1.13–2.31] mGy s^{-1} used for the measurements of this work have been measured through a BARRACUDA X-Ray Analyzer.

RESULTS AND DISCUSSION

Different types of measurements have been performed in order to test the reliability of the detector for medical monitoring and diagnostic analysis conditions.

Figure 2 shows the normalized signal amplitude variation of the four pixels measured for subsequent synchrotron 17 keV X-rays on/off cycles (2 s on and 10 s off) for different thicknesses of Aluminum filter, i.e., different dose rates. In particular, 0.50, 0.75, and 1 mm Al thick filters were used, corresponding to 17.1, 12.1, 8.1 mGy s^{-1} dose rates impinging on the detector, respectively. The normalized signal amplitude variation has been calculated as $(\Delta I_i - \Delta I_1)/\Delta I_1$ where ΔI_i = Ion-Ioff is the X-ray induced photocurrent of the ith exposure to X-rays. The orange dashed line indicates the average value, weighted with the squared reverse of standard deviation associated to each pixel. The error band has been calculated as 3 times the associated error (99.7% accuracy), i.e., the sum of the squared reverse of standard deviation associated to each pixel. Also, the linear fits of each set of data are also reported as negative slope solid lines in the graph. The results show that for all the pixels, even if a progressive

degradation of the response amplitude can be noticed, it remains within 20% of the value recorded for the first irradiation cycle. Noteworthy, the signal stability is higher for lower doses, in fact the response variation remains below 12% for all the pixels at 8.1 mGy s^{-1}, a promising feature for medical diagnostic application, where typically low doses (from few mGy to μGy) are used. This feature is further clearly shown by the progressive slope reduction of the linear fits of the data with decreasing of the dose rate. In fact, such a degradation is due to a lag effect, i.e., the drifting of the baseline due to the previous irradiation, and reduces below 3% at 5.30 mGy s^{-1} and shorter exposure (500 ms instead of 2 s) as will be shown later on. Further, since the progressive reduction of the X-ray induced photocurrent amplitude is ruled by the hole/electron recombination dynamics after the X-ray exposure [16, 25], it is a reversible effect at least for the doses typically used in medical diagnostic analysis. In fact, by exposing the detector to strong X-ray irradiation (see **Supplementary Information**), we could assess a degradation of 56% after a total dose of 750 Gy, delivered in four steps of 250 Gy waiting 10 min between steps. After 100 h rest in dark at room temperature, a recovery of the signal to a value which is almost equal to that of the previous irradiation step is observed, meaning that such radiation damage is, at least partially, reversible. It is noteworthy that the X-ray doses employed for such radiation hardness tests are very high if compared to typical dose delivered to a patient during a medical diagnostic analysis (for example for a chest radiography it is about 12 μGy).

We first assessed the potential usage of organic thin film detectors as medical dosimeters able to measure the density of a phantom placed between the X-rays source and the device. Polytetrafluoroethylene (PTFE), or Teflon, is a material commonly used in orthopedic surgery since its density (about 2.25 g cm^{-3}) is similar to that of human bones (1.92 g cm^{-3} for cortical bone) [43]. Therefore, in order to assess the reliability of

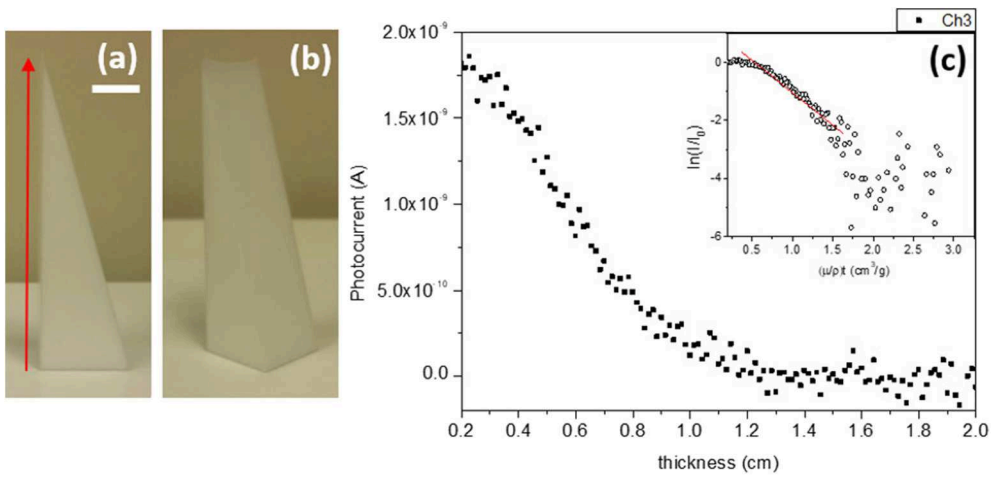

FIGURE 3 | Picture of the Teflon wedge, side view **(a)** and oblique view **(b)**. The red arrow indicates the scanning direction of the phantom in front of the detector. The scale bar is 1 cm. **(c)** Photocurrent in function of the wedge thickness. In inset the logarithmic plot and the correspondent linear fit (red line).

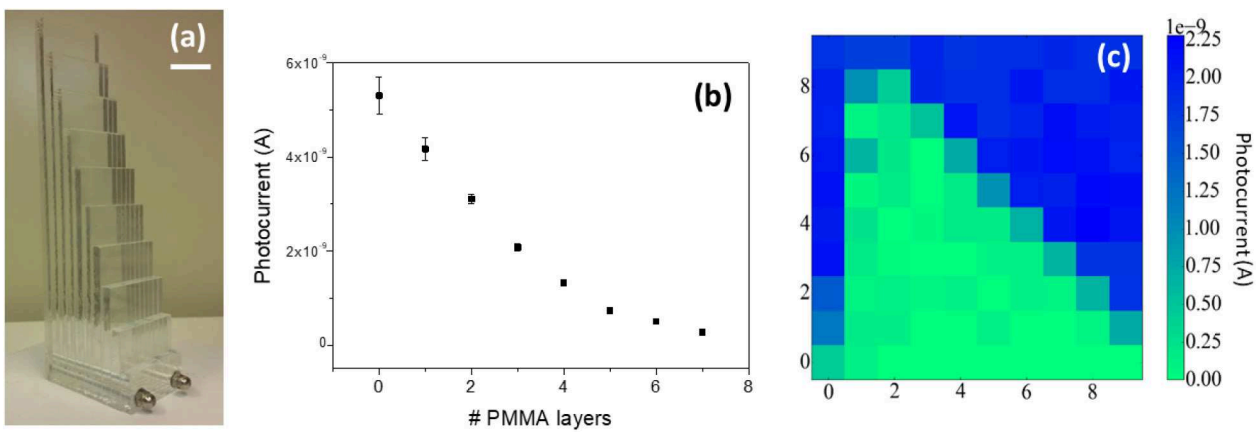

FIGURE 4 | (a) PMMA mammographic phantom (scale bar 15 mm). **(b)** Photocurrent response for the different numbers of PMMA steps. **(c)** X-ray image of the PMMA phantom profile.

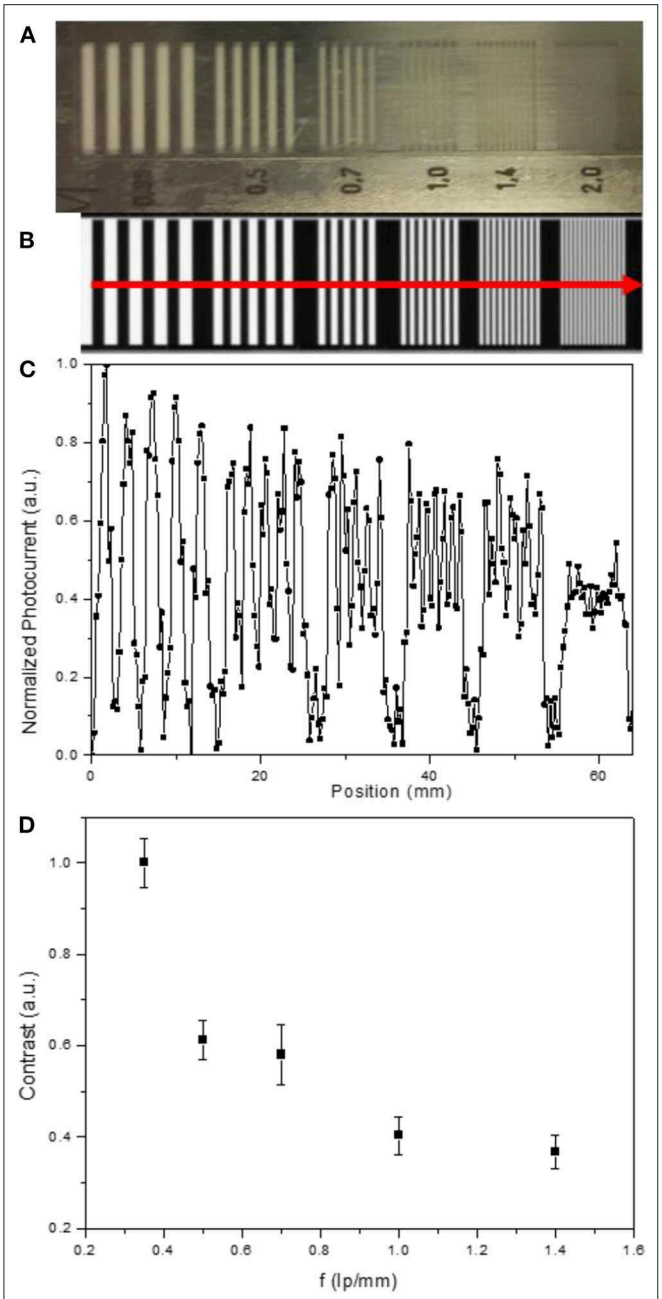

FIGURE 5 | (A) Bar space pattern used to calculate the intensity contrast of the detector and **(B)** correspondent image from a CCD, the red arrow represents the scanning direction of the phantom. **(C)** Normalized photocurrent signal recorded by sweeping the pattern in front of the detector. **(D)** Correspondent Contrast vs. spatial frequency plot.

the detector for widespread medical diagnostic analyses, e.g., as bone density analyzer for the diagnostic of several osteoarticular diseases, the X-rays absorbance profile of a Teflon wedge has been measured. **Figures 3a,b** show a picture of the Teflon wedge, side view and oblique view, respectively. The X-ray induced photocurrent profile, measured by moving the phantom in front of the detector from the base to the top of the wedge (red arrow in **Figure 3a**), and obtained by means of 140 X-ray exposures, is reported in **Figure 3c**. The photocurrent is directly proportional to the intensity I of the transmitted X-ray beam, that follows the exponential attenuation law:

$$\frac{I}{I_0} = e^{-\frac{\mu}{\rho}x} \tag{1}$$

Where I_0 is the total X-ray beam intensity impinging onto the phantom, μ/ρ is the mass attenuation coefficient, $x = \rho t$ is the mass thickness, i.e., the mass per unit area, with ρ and t indicating the density and the thickness, respectively. The Teflon mass attenuation coefficient for 17 keV X-rays can be found in the NIST database [44], and results about 1.48 $cm^2\ g^{-1}$. Since Equation (1) can be written as:

$$\ln\left(\frac{I}{I_0}\right) = -\rho\left(\frac{\mu}{\rho}\right)t \tag{2}$$

the material density can be found as the slope of the linear fit of the plot of $\ln(I/I_0)$ vs. $(\mu/\rho)t$, reported in the inset of **Figure 3c**. The resulting density averaged for 3 different devices is: (2.27 ± 0.07) g cm^{-3}. The reference Teflon density value of 2.25 g cm^{-3} [43] is therefore comparable to the measured mean value within the error. The consistency of the measured material density with the nominal one demonstrates the potential of organic X-ray detectors as innovative wearable personal dosimeter for medical analyses, for example to be employed as bone-density analyzer, where two detectors, one in the front of the patient and the second behind the bone, could acquire a real-time differential signal. The employment of monochromatic synchrotron radiation is essential for such an assessment since it allows an accurate estimation of the μ/ρ values.

Further, we measured at SYRMEP the X-rays response of the organic detectors to test their performance as medical personal dosimeter using a mammographic phantom (**Figure 4a**), made of Poly(methyl methacrylate) (PMMA) absorption steps. For each PMMA step, 5 acquisitions have been measured and the results are plotted in **Figure 4b**. All the pixels properly respond to the different radiation intensities at 17 keV, the typical mean energy value employed in mammographic X-ray system. It should be noted that by reducing the intensity of the impinging X-rays, i.e., by increasing the number of PMMA steps, the detector response to the transmitted X-rays reduces its slopes. However, the linearity of the response for low doses has been also assessed (see after). The profile image of the phantom was also acquired, achieving the 13 × 13 X-ray image reported in **Figure 4c**. The image was obtained by moving the phantom of 1 pixel size length 4 mm in x direction and of 1 cm in y direction, the phantom profile is clearly distinguishable from the background giving the proof of principle for the possible employment of organic detectors as X-rays imagers.

With the aim to better assess the detector performance as a medical imager we used a bar space pattern to evaluate the achievable image contrast. **Figure 5A** shows the bar space pattern (**Figure 5B** reports the correspondent image from

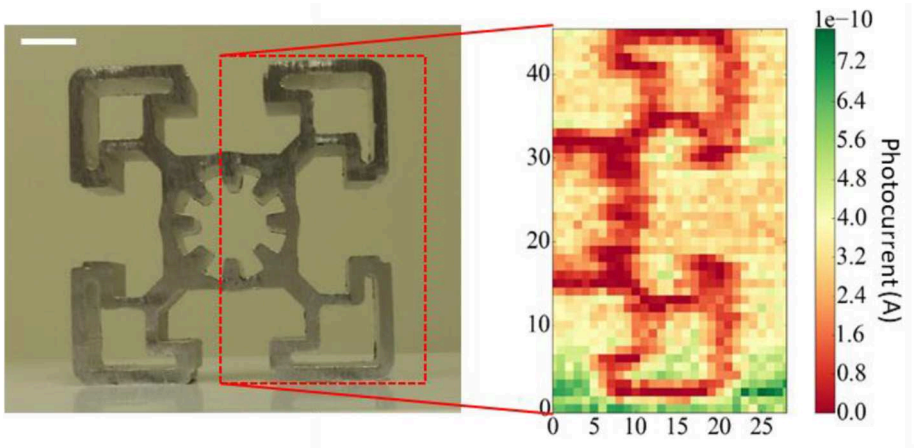

FIGURE 6 | Photograph **(left)** and corresponding X-ray image by a single pixel device **(right)** of an aluminum object. The red dashed box indicates the portion of the object scanned by the detector. The scale bar is 1 cm.

the CCD) used to calculate the spatial resolution of the detector. The profile is obtained under a not filtered 17 keV synchrotron X-ray beam, shaped with the dimension of (1 × 16 mm) through the slits provided by the beamline, by sweeping the pattern in front of and throughout the detector (following the red arrow reported in **Figure 5B**). Such profile allows computing the contrast obtained for each spatial frequency. The contrast has been calculated through the equation:

$$Contrast = \frac{I_{MAX} - I_{MIN}}{I_{MAX} + I_{MIN}} \quad (3)$$

Where I_{MAX} and I_{MIN} are the maximum/minimum current values under irradiation/dark conditions (**Figure 5C**), for each spatial frequency. The plot of the contrast obtained from the response of our detector vs. the spatial frequency is reported in **Figure 5D**. With the experimental conditions described above we could observe 1.4 lp mm^{-1} with a contrast of 0.37. In **Figure 5C** also the pattern for 2lp mm^{-1} is reported. The signal peaks are barely visible at this resolution due to the size of the sample, thus a reliable calculation of the contrast is not possible, but it can be considered a potential value for this kind of technology after a proper sizing of the pixels. To the best of our knowledge, only a couple of works in literature report a similar analysis on an organic-based detector: one is that of Büchele et al. [45], reporting a resolution of 4.75 lp mm^{-1} at a modulated transfer function MTF = 0.2, and more recently Jayawardena et al. [46] assessed resolution of about 1 lp mm^{-1} at MTF = 0.2. It is noteworthy that in both these cases the resolution was determined via slanted edge method while we used a bar space pattern, therefore the here obtained contrast is not directly comparable to the MTF reported in literature but it can be considered as a potential imaging performance achievable by proper scaling of the system. Moreover, the hybrid/organic photo-active layer of the detectors reported in Tromba et al. [41] and Dreossi et al. [42] is deposited over a rigid a-Si:H TFT array backplane, therefore the devices remain heavy, stiff and not transparent to the X-rays, i.e., completely different from the here reported direct flexible, lightweight, tissue-like fully organic detector, that operate without any kind of TFT-based structure behind it.

To further proof the reliability of the detector and to show its potential as a X-ray imager, we acquired an image of a structured Aluminum profile (**Figure 6**, left), obtaining good image quality and high contrast of the 2 mm features (**Figure 6**, right). The resulting image has been acquired by single pixel measurement, under a 17 keV monochromatic X-ray beam, filtered by a 0.75 mm thick aluminum slice, scanning the object in y and in x directions with 1 mm step, corresponding to 1,260 acquisitions (28 × 45 pixels). Even if the commercial flat panel performances are still far, by a proper optimization of the system and an appropriate design and sizing of the pixel, a good large area imager can be obtained, that can be exploited also for other non-medical applications, e.g., security and luggage inspection, where sub-millimeter resolution is sufficient to achieve the information of interest. It is noteworthy that scalability of electronic devices onto flexible substrate has been largely demonstrated in literature. Sun et al. [47] quite recently reported about fully printed organic devices through a scalable printing method, such as a roll-to-roll (R2R) gravure. They fabricated full R2R gravure printed 20 × 20 Organic TFT active matrices onto 100 μm thick PET web by employing four different commercially available organic semiconductors, including TIPS-pentacene. They reached 10 PPI resolution, more than 98% device yield and 50% electrical variation along 10 m of PET web.

Among the several widespread applications where the lightweight, low operating bias and mechanical flexibility of the here reported organic thin-film detector could be exploited, we chose to explore their potential in dental radiography applications, that require higher X-ray energies (peak kilovoltage of 70 kVp), lower irradiation doses (few μGy) and short

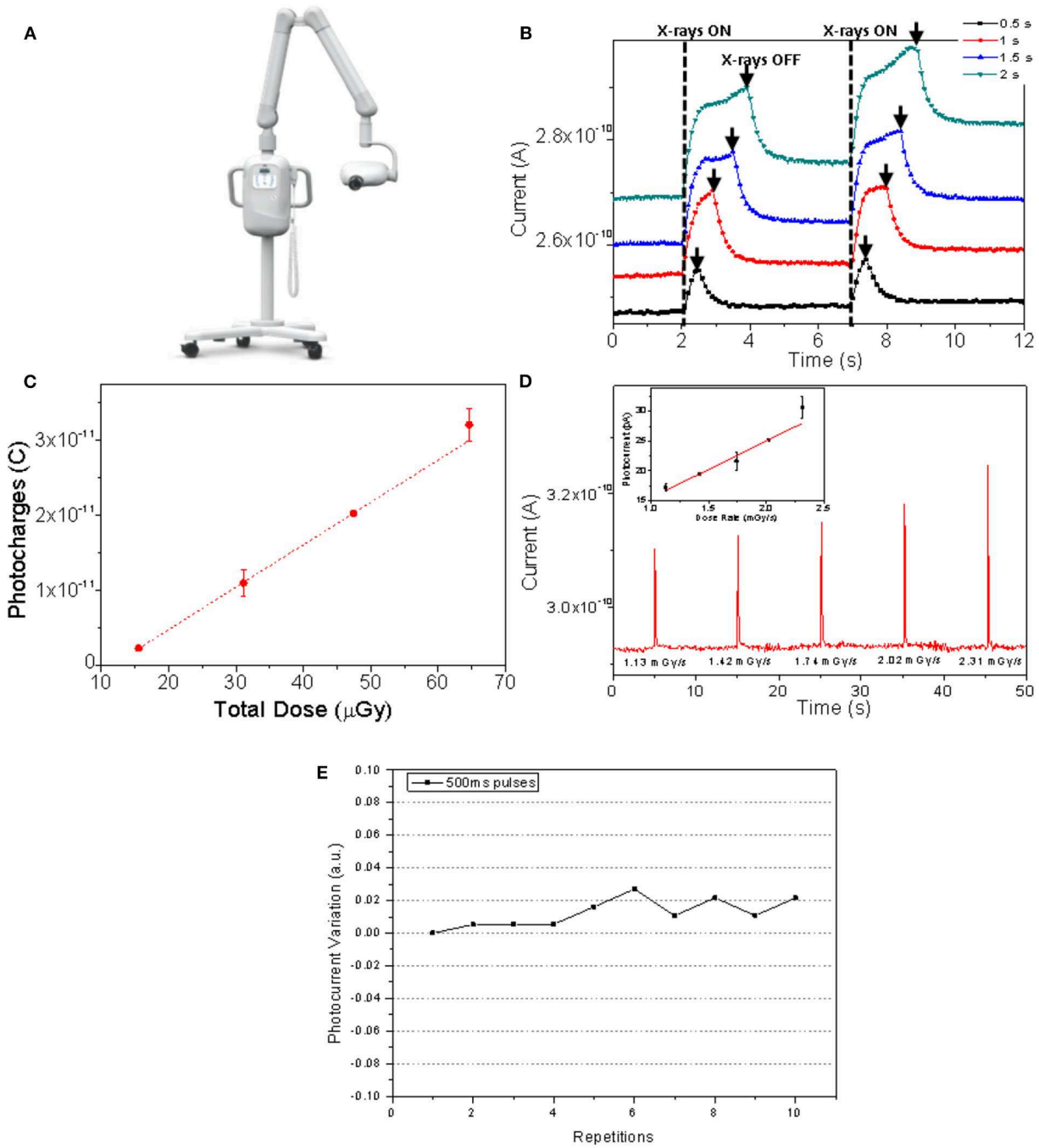

FIGURE 7 | (A) Intraskan DC, Skanray dental radiography system. **(B)** Current response of the detector to the X-ray beam provided by a W-target X-ray tube operated at 70 kVp accelerating voltage and 4 mA filament current, for different exposition time windows: 0.5, 1, 1.5, 2 s. The vertical black dashed lines indicate when the X-ray tube is turned on while the black arrows when it is switched off. **(C)** Plot of the corresponding generated photocharges in function of the total dose impinged on the detector for the different exposure times. **(D)** Dynamic signal response to 100 ms X-rays pulses at different dose rates provided by the Intraskan DC machine. In inset the corresponding plot of X-ray induced photocurrent in function of the dose rate. **(E)** Normalized signal amplitude variation for 500 ms X-ray pulses exposure over 10 repetitions.

irradiation pulses (hundreds of ms). We tested the detectors using commercial irradiation sources for dental radiography:

1) W-target X-ray tube operated at 70 kVp accelerating voltage and 4 mA anodic current. By varying the exposure time in the window [0.5 −2] s, corresponding of irradiation doses in the range [15.5–64.6] μGy.
2) A commercial dental radiography system, i.e., Intraskan DC, Skanray (**Figure 7A**, see Experimental section for details), to

test the device under the actual operating conditions, i.e., energy of 70 keV, pulse width 100 ms, and dose rates in the range [1.13–2.31] mGy s^{-1}. In this case the dose rates were varied by changing the anodic current in the range [4–8] mA.

In **Figure 7B**, the dynamic responses for 0.5, 1, 1.5, 2 s of irradiation at 70 kVp from the W-target X-ray tube are reported. In this case, the X-ray flux is kept constant by setting the current at 4 mA, therefore decreasing the exposure time leads to the decrease of the total dose impinging on the detector. The dynamical response to X-rays is the one typical of organic thin films-based devices and it is clearly distinguishable from the background down to 15.5 μGy of total dose. By calculating the amount of charges generated in the organic layer by the interaction with the radiation as the integral of the current vs. time curves reported in **Figure 7B**, it is possible to plot the photo-generated charge in function of the total X-rays dose (**Figure 7C**). From the slope of the linear fit of the so obtained experimental points, a sensitivity of 1.6×10^5 μC Gy^{-1} cm^{-3} has been obtained, a value in-line with that reported for analogous devices considering the detector structures [25] and the organic semiconductor employed [34], characterized at much higher X-ray doses and lower energies (5–30 mGy s^{-1}; 35 keV). Moreover, in order to test the detector performance under short pulses of X-rays and to validate it in actual measurement condition for medical imaging application, we expose it to a pulsed X-ray beam (duration 100 ms) provided by a commercial dental radiography system, i.e., Intraskan DC, Skanray, as mentioned above. The detectors respond to the 100 ms X-ray pulses with clean and steep output signals with an amplitude proportional to the impinging dose rate (see the linear regression of the photocurrent vs. dose rates in inset of **Figure 7D**), demonstrating to be able to follow the typical frame rates of a commercial dental radiographic apparatus. Further, from the baseline of the measurement reported in **Figure 7D** we could calculate the noise of the system as three times the root mean square of the experimental data, obtaining the value of 1.5 pA. Combining this value with the plot of X-ray induced photocurrent in function of the dose rate reported in the inset of the **Figure 7D**, we could derive the lowest detectable dose of about 12 μGy (see **Supplementary Information** for detail). Noteworthy, as previously mentioned, working at low doses and short pulses strongly reduces the lag effect and, therefore, improves the signal stability, with a deviation of 2.7% for 10 subsequent repetitions of 500 ms X-rays exposure (**Figure 7E**).

CONCLUSIONS

In this paper we provide the characterization and assessment of full-organic, tissue-equivalent flexible direct X-ray detectors, operating at voltages below 1 V and therefore suitable for the developing of wearable sensing systems, in actual clinical environment for medical diagnostic and dosimetry applications. The detector demonstrates reliable performance as dosimeter, measuring the density of a Teflon phantom in accordance to the nominal value within the experimental error. Also, the proper response of the detector employing an actual mammographic phantom has been assessed. To envisage its potential use as X-ray imager for medical diagnostic application, the X-ray images of an actual mammographic phantom and of a structured Aluminum profile were acquired, and a resolution of 1.4 lp mm^{-1} with a contrast of 0.37 has been estimated. Further, by means of tests under commercial dental X-ray panoramic tube and dental radiography machine we could verify the linear and highly reproducible response to the actual dose rates and time pulses typical of such radiography analyses, with a sensitivity of 1.6×10^5 μC Gy^{-1} cm^{-3} and a deviation of 2.7% for 10 subsequent repetitions of 500 ms X-rays exposure. This value is very close to the typical deviation of about 2.5% for a-Si detectors employed for dental radiography. Finally, the detector ability to follow 100 ms X-ray pulses, with a signal amplitude directly proportional to the X-ray dose rates delivered has been also proved.

DATA AVAILABILITY STATEMENT

The datasets generated for this study are available on request to the corresponding author.

AUTHOR CONTRIBUTIONS

LB and AC conceived the experiments, performed the measurements at SYRMEP beamline, and analyzed the data. AC and IF performed the measurements with the Intraskan DC radiography system, and analyzed the data. LB, AC, and IF also contributed to the device fabrication with the deposition of organic semiconductor. DD and GT gave hardware and software technical support during the experiments at the synchrotron ELETTRA. FM, VB, and CD performed and managed the measurements with the OPX/105 tube at Skan-X Radiology Devices S.p.A. SL, PC, and AB conceived and fabricated the devices. JA synthetized the organic semiconducting small molecules employed as active layer of the detectors. LB wrote the first draft of the manuscript. All authors discussed the results and revised the manuscript. BF coordinated the project.

ACKNOWLEDGMENTS

LB, AC, IF, and BF acknowledge funding from INFN through the CSN5 FIRE project. JA thanks the U.S. National Science Foundation (DMREF-1627428) for support of material synthesis.

SUPPLEMENTARY MATERIAL

The Supplementary Material for this article can be found online at: https://www.frontiersin.org/articles/10.3389/fphy.2020.00013/full#supplementary-material

Supplementary Figure 1 | Radiation hardness measurements: the X-ray induced photocurrent has been measured after four irradiation steps of 250Gy each. At the end of the four irradiation steps, the detectors were stored in dark for 100 hours at room temperature and then again characterized.

Supplementary Figure 2 | Plot of X-ray induced photocurrent in function of the dose rate, where the blue star indicates the lowest detectable dose rate.

REFERENCES

1. Bruzzi M, Bucciolini M, Cirrone GAP, Cuttone G, Guasti A, Mazzocchi S, et al. Characterization of CVD diamond films as radiation detectors for dosimetric applications. *IEEE Trans Nuclr Sci.* (2000) **47**:1430–3. doi: 10.1109/23.872991
2. Fraboni B, Ciavatti A, Merlo F, Pasquini L, Cavallini A, Quaranta A, et al. Organic semiconducting single crystals as next generation of low-cost, room-temperature electrical X-ray detectors. *Adv Mater.* (2012) **24**:2289–93. doi: 10.1002/adma.201200283
3. Basirico L, Ciavatti A, Sibilia M, Fraleoni-Morgera A, Trabattoni S, Sassella A, et al. Solid state organic X-ray detectors based on rubrene single crystals. *IEEE Trans Nucl Sci.* (2015) **62**:1791–7. doi: 10.1109/TNS.2015.2456418
4. Mills CA, Intaniwet A, Shkunov M, Keddie JL, Sellin PJ. Flexible radiation dosimeters incorporating semiconducting polymer thick films. In: *Proceedings Volume 7449, Hard X-Ray, Gamma-Ray, and Neutron Detector Physics.* San Diego, CA (2009). p. 74491I—7.
5. Intaniwet A, Mills CA, Shkunov M, Thiem H, Keddie JL, Sellin PJ. Characterization of thick film poly(triarylamine) semiconductor diodes for direct x-ray detection. *J Appl Phys.* (2009) **106**:064513. doi: 10.1063/1.3225909
6. Intaniwet A, Keddie JL, Shkunov M, Sellin PJ. High charge-carrier mobilities in blends of poly(triarylamine) and TIPS-pentacene leading to better performing X-ray sensors. *Organ Electron.* (2011) **12**:1903–8. doi: 10.1016/j.orgel.2011.08.003
7. Ciavatti A, Sellin PJ, Basiricò L, Fraleoni-Morgera A, Fraboni B. Charged-particle spectroscopy in organic semiconducting single crystals. *Appl Phys Lett.* (2016) **108**:153301. doi: 10.1063/1.4945597
8. Gelinck GH, Kumar A, Moet D, van Steen J-LPJ, van Breemen AJJM, Shanmugam S, et al. X-ray detector-on-plastic with high sensitivity using low cost, solution-processed organic photodiodes. *IEEE Trans Electr Dev.* (2016) **63**:197–204. doi: 10.1109/TED.2015.2432572
9. Gelinck GH, Kumar A, Moet D, van der Steen J-L, Shafique U, Malinowski PE, et al. X-ray imager using solution processed organic transistor arrays and bulk heterojunction photodiodes on thin, flexible plastic substrate. *Organ Electr.* (2013) **14**:2602–9. doi: 10.1016/j.orgel.2013.06.020
10. Diao Y, Tee BC-K, Giri G, Xu J, Kim DH, Becerril HA, et al. Solution coating of large-area organic semiconductor thin films with aligned single-crystalline domains. *Nat Mater.* (2013) **12**:665–71. doi: 10.1038/nmat3650
11. Tedde SF, Kern J, Sterzl T, Fürst J, Lugli P, Hayden O. Fully spray coated organic photodiodes. *Nano Lett.* (2009) **9**:980–3. doi: 10.1021/nl803386y
12. Minemawari H, Yamada T, Matsui H, Tsutsumi J, Haas S, Chiba R, et al. Inkjet printing of single-crystal films. *Nature.* (2011) **475**:364–7. doi: 10.1038/nature10313
13. Christophorou LG, Carter JG. Improved organic scintillators in 2-ethyl naphthalene. *Nature.* (1966) **212**:816–8. doi: 10.1038/212816a0
14. Takada E, Fujii K, Imai H, Okada H, Namito Y, Nakamura T. Response of organic photodiode fabricated directly on plastic scintillator to X-rays. *J Nucl Sci Technol.* (2015) **52**:104–8. doi: 10.1080/00223131.2014.933135
15. Hull G, Zaitseva NP, Cherepy NJ, Newby JR, Stoeffl W, Payne SA. New organic crystals for pulse shape discrimination. *IEEE Trans Nucl Sci.* (2009) **56**:899–903. doi: 10.1109/TNS.2009.2015944
16. Baeg K-J, Binda M, Natali D, Caironi M, Noh Y-Y. Organic light detectors: photodiodes and phototransistors. *Adv Mater.* (2013) **25**:4267–95. doi: 10.1002/adma.201204979
17. Binda M, Natali D, Sampietro M, Agostinelli T, Beverina L. Organic based photodetectors: Suitability for X- and Γ-rays sensing application. *Nucl Instrum Methods Phys Res Sect A.* (2010) **624**:443–8. doi: 10.1016/j.nima.2010.04.026
18. Ciavatti A, Capria E, Fraleoni-Morgera A, Tromba G, Dreossi D, Sellin PJ, et al. Toward low-voltage and bendable x-ray direct detectors based on organic semiconducting single crystals. *Adv Mater.* (2015) **27**:7213–20. doi: 10.1002/adma.201503090
19. Carman L, Martinez HP, Voss L, Hunter S, Beck P, Zaitseva N, et al. Solution-grown rubrene crystals as radiation detecting devices. *IEEE Trans Nucl Sci.* (2017) **64**:781–8. doi: 10.1109/TNS.2017.2652139
20. Pipan G, Bogar M, Ciavatti A, Basiricò L, Cramer T, Fraboni B, et al. Direct inkjet printing of TIPS-pentacene single crystals onto interdigitated electrodes by chemical confinement. *Adv Mater Interfaces.* (2017) **5**:1700925. doi: 10.1002/admi.201700925
21. Fraboni B, Fraleoni-Morgera A, Zaitseva N. Ionizing radiation detectors based on solution-grown organic single crystals. *Adv Funct Mater.* (2015) **26**:2276–91. doi: 10.1002/adfm.201502669
22. Fraboni B, Ciavatti A, Basiricò L, Fraleoni-Morgera A. Organic semiconducting single crystals as solid-state sensors for ionizing radiation. *Faraday Discuss.* (2014) **174**:219–34. doi: 10.1039/C4FD00102H
23. Thirimanne HM, Jayawardena KDGI, Parnell AJ, Bandara RMI, Karalasingam A, Pani S, et al. High sensitivity organic inorganic hybrid X-ray detectors with direct transduction and broadband response. *Nat Commun.* (2018) **9**:2926. doi: 10.1038/s41467-018-05301-6
24. Intaniwet A, Mills CA, Sellin PJ, Shkunov M, Keddie JL. Achieving a stable time response in polymeric radiation sensors under charge injection by X-rays. *ACS Appl Mater Interfaces.* (2010) **2**:1692–9. doi: 10.1021/am100220y
25. Basiricò L, Ciavatti A, Cramer T, Cosseddu P, Bonfiglio A, Fraboni B. Direct X-ray photoconversion in flexible organic thin film devices operated below 1 V. *Nat Commun.* (2016) **7**:13063. doi: 10.1038/ncomms13063
26. Lai S, Cosseddu P, Basiricò L, Ciavatti A, Fraboni B, Bonfiglio A. A highly sensitive, direct X-ray detector based on a low-voltage organic field-effect transistor. *Adv Electron Mater.* (2017) **3**:1600409. doi: 10.1002/aelm.201600409
27. Intaniwet A, Mills CA, Shkunov M, Sellin PJ, Keddie JL. Heavy metallic oxide nanoparticles for enhanced sensitivity in semiconducting polymer x-ray detectors. *Nanotechnology.* (2012) **23**:235502. doi: 10.1088/0957-4484/23/23/235502
28. Mills CA, Al-Otaibi H, Intaniwet A, Shkunov M, Pani S, Keddie JL, et al. Enhanced x-ray detection sensitivity in semiconducting polymer diodes containing metallic nanoparticles. *J Phys D.* (2013) **46**:275102. doi: 10.1088/0022-3727/46/27/275102
29. Ciavatti A, Cramer T, Carroli M, Basiricò L, Fuhrer R, De Leeuw DM, et al. Dynamics of direct X-ray detection processes in high-Z Bi2O3 nanoparticles-loaded PFO polymer-based diodes. *Appl Phys Lett.* (2017) **111**:183301. doi: 10.1063/1.4986345
30. Ankah GN, Büchele P, Poulsen K, Rauch T, Tedde SF, Gimmler C, et al. PbS quantum dot based hybrid-organic photodetectors for X-ray sensing. *Organ Electron.* (2016) **33**:201–6. doi: 10.1016/j.orgel.2016.03.023
31. Yakunin S, Sytnyk M, Kriegner D, Shrestha S, Richter M, Matt GJ, et al. Detection of X-ray photons by solution-processed lead halide perovskites. *Nat Photon.* (2015) 9:444–9. doi: 10.1038/nphoton.2015.82
32. Basiricò L, Senanayak SP, Ciavatti A, Abdi-Jalebi M, Fraboni B, Sirringhaus H. Detection of X-rays by solution-processed cesium-containing mixed triple cation perovskite thin films. *Adv Funct Mater.* (2019) **29**:1902346. doi: 10.1002/adfm.201902346
33. Gill HS, Elshahat B, Kokil A, Li L, Mosurkal R, Zygmanski P, et al. Flexible perovskite based X-ray detectors for dose monitoring in medical imaging applications. *Phys Med.* (2018) **5**:20–3. doi: 10.1016/j.phmed.2018.04.001
34. Ciavatti A, Basiricò L, Fratelli I, Lai S, Cosseddu P, Bonfiglio A, et al. Boosting direct X-ray detection in organic thin films by small molecules tailoring. *Adv Funct Mater.* (2019) **29**:1806119. doi: 10.1002/adfm.201806119
35. Kabir MZ, Kasap S. Photoconductors for X-ray image detectors. In: Kasap S, Capper P, editors. *Springer Handbook of Electronic and Photonic Materials Springer Handbooks*. Cham: Springer International Publishing (2017). p. 1. doi: 10.1007/978-3-319-48933-9_45
36. Boroumand FA, Zhu M, Dalton AB, Keddie JL, Sellin PJ. Direct x-ray detection with conjugated polymer devices. *Appl Phys Lett.* (2007) **91**:033509. doi: 10.1063/1.2748337
37. *CRC Handbook of Chemistry and Physics, 100th Edition*. CRC Press Available online at: https://www.crcpress.com/CRC-Handbook-of-Chemistry-and-Physics-100th-Edition/Rumble/p/book/9781138367296 (accessed November 29, 2019).
38. Hong J-P, Park A-Y, Lee S, Kang J, Shin N, Yoon DY. Tuning of Ag work functions by self-assembled monolayers of aromatic thiols for an efficient hole injection for solution processed triisopropylsilylethynyl pentacene organic thin film transistors. *Appl Phys Lett.* (2008) **92**:143311. doi: 10.1063/1.2907691
39. Jain S, Surya SG, Suggisetti PK, Gupta A, Rao VR. Sensitivity improvement of medical dosimeters using solution processed TIPS-Pentacene FETs. *IEEE Sens J.* (2019) **19**:4428–34. doi: 10.1109/JSEN.2019.2901810
40. Glenn F. Knoll. *Radiation Detection and Measurements*. 4th ed. John Wiley & Sons, Inc. (2011).

41. Tromba G, Longo R, Abrami A, Arfelli F, Astolfo A, Bregant P, et al. The SYRMEP Beamline of Elettra: clinical mammography and bio-medical applications. *AIP Conf Proc.* (2010) **1266**:18–23. doi: 10.1063/1.3478190
42. Dreossi D, Abrami A, Arfelli F, Bregant P, Casarin K, Chenda V, et al. The mammography project at the SYRMEP beamline. *Eur J Radiol.* (2008) **68**:S58–62. doi: 10.1016/j.ejrad.2008.04.038
43. Pronyaev VG. XMuDat: *Photon attenuation data on PC. Version 1.0.1 of August 1998. Summary Documentation*. International Atomic Energy Agency (1998). Available online at: http://inis.iaea.org/Search/search.aspx?orig_q=RN:30022813 (accessed September 12, 2019).
44. Berger MJ, Hubbell JH, Seltzer SM, Chang J, Coursey JS, Sukumar R, et al. *XCOM: Photon Cross Sections Database*. (2015). Available online at: http://www.nist.gov/pml/data/xcom/index.cfm (accessed January 3, 2015).
45. Büchele P, Richter M, Tedde SF, Matt GJ, Ankah GN, Fischer R, et al. X-ray imaging with scintillator-sensitized hybrid organic photodetectors. *Nat Photon.* (2015) **9**:843–8. doi: 10.1038/nphoton.2015.216
46. Jayawardena KDGI, Thirimanne HM, Tedde SF, Huerdler JE, Parnell AJ, Bandara RMI, et al. Millimeter-scale unipolar transport in high sensitivity organic–inorganic semiconductor X-ray detectors. *ACS Nano*. (2019) **13**:6973–81. doi: 10.1021/acsnano.9b01916
47. Sun J, Park H, Jung Y, Rajbhandari G, Maskey BB, Sapkota A, et al. Proving scalability of an organic semiconductor to print a TFT-active matrix using a roll-to-roll gravure. *ACS Omega.* (2017) **2**:5766–74. doi: 10.1021/acsomega.7b00873

Conflict of Interest: FM and CD were employed by the company Skan-X Radiology Devices S.p.A., Bologna, Italy. VB was employed by the company Skanray Europe S.r.l., Bologna, Italy.

The remaining authors declare that the research was conducted in the absence of any commercial or financial relationships that could be construed as a potential conflict of interest.